Journal of Radioanalytical and Nuclear Chemistry
https://doi.org/10.1007/s10967-019-06844-8

# Production of $^{47}$Sc with natural vanadium targets: results of the PASTA project

Gaia Pupillo[1] · Liliana Mou[1] · Alessandra Boschi[2] · Simone Calzaferri[3,4] · Luciano Canton[5] · Sara Cisternino[1] · Lucia De Dominicis[6] · Adriano Duatti[2] · Andrea Fontana[4] · Férid Haddad[7,8] · Petra Martini[1] · Micòl Pasquali[1] · Hanna Skliarova[1] · Juan Esposito[1]

Received: 31 July 2019


**Abstract**
The goal of PASTA project (acronym for production with accelerator of $^{47}$Sc for theranostic applications) is the determination of excitation functions associated to several nuclear reactions, aimed at yielding the theranostic radionuclide $^{47}$Sc. This work reports the main results obtained by irradiating natural vanadium targets with proton beams up to 70 MeV. Particular care is also given to the co-production of $^{46}$Sc, the only isotopic contaminant with half-life longer than $^{47}$Sc. Experimental results are compared with theoretical studies by means of known nuclear reaction software tools that are publicly available.

**Keywords** $^{47}$Sc · Theranostic radionuclides · Proton-induced reactions · Cyclotron-induced reactions · $^{46}$Sc · Nuclear reaction codes

## Introduction

The production of $^{47}$Sc has been investigated for more than 40 years [1] and it is recently achieving new attention from the international community, as underlined by the ongoing Coordinated Research Project (CRP) promoted by the International Atomic Energy Agency (IAEA), focused on the study of *Therapeutic Radio-pharmaceuticals Labeled with New Emerging Radionuclides* ($^{67}$*Cu*, $^{186}$*Re*, $^{47}$*Sc*) [2]. This renewed interest on $^{47}$Sc is based on the possibility to pair it with a $\beta^+$ emitter isotope (such as $^{44g}$Sc, $^{44m}$Sc and $^{43}$Sc) to obtain a multi-use $^{4x}$Sc-labelled radiopharmaceutical for theranostic purposes, i.e. a chemically-identical molecule with the same kinetic properties for diagnosis and therapy [3]. PET/CT studies prior therapy allows not only for patients' selection with a good response to specific pharmacokinetics, but also to tailor the dose to patient's needs. The $^{47}$Sc intense $\beta^-$ radiation (mean energy 162.0 keV, 100%) is useful to deliver cytotoxic doses to small-medium sized tumors [4]. Moreover, during the treatment, the tumor uptake through SPECT imaging may be also followed, by exploiting its γ-emission (159.381 keV, 68.3%). In addition, the long half-life of $^{47}$Sc (3.3492 d) permits to follow the slow biodistribution of large molecules, including the monoclonal antibodies used in radioimmuno therapy.

The versatile chemistry of the third group of the periodic table elements such as Sc-isotopes, that can be easily separated from irradiated target applying efficient separation and purification methods [5, 6], opens up new possibilities for the development of innovative radiopharmaceuticals based on the use of these promising radiometals. For all these

✉ Gaia Pupillo
gaia.pupillo@lnl.infn.it

1 Laboratori Nazionali di Legnaro (LNL), Istituto Nazionale di Fisica Nucleare (INFN), Viale dell'Università 2, 35020 Legnaro, PD, Italy

2 Dip.to di Scienze Chimiche e Farmaceutiche and Sezione INFN di Ferrara, Università degli Studi di Ferrara, Via G. Saragat 1, 44122 Ferrara, FE, Italy

3 Dip.to di Fisica, Università degli Studi di Pavia, Via A. Bassi, 6, 27100 Pavia, PV, Italy

4 Sezione INFN di Pavia, Via A. Bassi 6, 27100 Pavia, PV, Italy

5 Sezione INFN di Padova, Via F. Marzolo 8, 35131 Padua, PD, Italy

6 Dip.to di Fisica, Università degli Studi di Bologna, Viale Berti Pichat 6/2, 40127 Bologna, BO, Italy

7 Subatech, CNRS/IN2P3, IMT Atlantique, Université de Nantes, CS 20722, 44307 Nantes Cedex, France

8 GIP ARRONAX, Rue Arronax 1, 44800 Saint-Herblain, France

Published online: 23 October 2019

reasons, $^{47}$Sc is of great potential in theranostic investigations and its production routes, including the photo-induced reactions and the ones provided by nuclear reactors, were recently reviewed [1]. However, despite the efforts to obtain high-quality $^{47}$Sc in enough amounts to broaden the encouraging results of the first preclinical studies [3], its production is still an open issue [2]. The PASTA project, funded by INFN at the National Laboratories of Legnaro (INFN-LNL) in 2017/2018, aims at studying several nuclear reactions of potential interest for $^{47}$Sc, to maximize its production while minimizing related contaminants. Considering the new 70 MeV high-performance, proton-cyclotron installed at the INFN-LNL and the dedicated LARAMED facility currently under development [7], the PASTA experimental program is focused on the nuclear reactions induced by proton beams only. In particular, the cross sections for the $^{47}$Sc production (and related contaminants) were measured by using $^{nat}$V and enriched $^{48}$Ti targets, in collaboration with the Arronax facility (Nantes, France) [8].

In this work the $^{nat}$V(p,x)$^{47}$Sc,$^{46}$Sc cross sections measured by using $^{nat}$V targets ($^{50}$V, 0.250% and $^{51}$V, 99.750%), a low-cost, easily available material, are reported. Particular attention is given to the co-production of $^{46}$Sc (83.79 d), since it is the only Sc contaminant having a longer half-life than $^{47}$Sc. In addition to the experimental tasks, the nuclear reactions of interest were also compared with the theoretical estimations obained by using different nuclear codes (TALYS, EMPIRE and FLUKA) [9–11]. The results of all the cross sections measured within the PASTA project will be published in a dedicated article.

## Experimental description

Six irradiation runs were carried out at the Arronax facility to perform stacked-foils experiments using the tunable (34–70 MeV) low current (100 nA) proton beam [12]. Thin $^{nat}$V foils (purity > 99.8%, thickness = 20 μm) were separated by thick aluminum foils, used as beam energy degrader. In order to measure the proton beam current through the stacked-foils target, a monitor (Ni foil for $E_P < 40$ MeV and Al foil for $E_P > 40$ MeV) was attached to each target foil. The $^{nat}$Ni(p,x)$^{57}$Ni and the $^{27}$Al(p,x)$^{24}$Na cross sections recommended by the IAEA (up-dated in 2017) [13] were considered as reference reactions in the data analysis, respectively for energies lower and higher than 40 MeV. The energy of the proton beam in each foil of the stacked-structure was calculated by using the software SRIM [14]. A HPGe detector, previously calibrated by using certified radioactive sources, was used to measure the activity of the radionuclides of interest by γ-spectrometry. The sample-detector distance was fixed at 19 cm to control the dead time during measurements. At least five acquisitions were carried out for each sample, in order to better follow the decay of the produced radionuclides. The first measurement of each $^{nat}$V foil started 2 h after the End of Bombardment (EOB) and was typically 15 min long; the following acquisitions, usually 3 h long, were performed once per day starting from the day after the EOB (up to 5 days). An additional acquisition of each sample was also carried out about 2 months after the EOB, to further measure the activity of the long-lived $^{46}$Sc. Data analysis, including uncertainty calculations, was performed for each spectrum by using the procedure described by Otuka et al. [15], taking into account the nuclear data from the NuDat 2.2 database [16] (Table 1). The final $^{nat}$V(p,x)$^{47}$Sc,$^{46}$Sc cross section value related to each target foil was calculated as the weighted average of all single values associated to each counting. The resulting uncertainty is thus smaller than those obtained through each single measurement. The uncertainty of the monitor cross section, reported in Table 3, is added at the end of this calculation.

## Theoretical calculations

Experimental data obtained in this work were compared with the previous ones available in the EXFOR database [17], and with calculations obtained with the reaction codes TALYS 1.9 [9], EMPIRE 3.2 [10], and FLUKA.dev.2018.0 [11]. The default set of parameters was used in the case of Empire and Fluka calculations. TALYS has a built-in variety of four models of pre-equilibrium and six models for nuclear level densities, for a total of 24 different combinations of models. The most widely adopted combination is the standard or default TALYS calculation, but alternative combinations of models can be applied. We have systematically studied in this mass region how the cross sections change in passing from one model to another, arriving at the conclusion that we could not plot the cross sections for all the 24 combinations of models because they would span a region too wide to be useful. Therefore, out of all the possibilities, we have selected a set of 10 TALYS model combinations (preeqmode = 1–2, ldmodel = 1–5) with similar behaviour. As a result, we obtained a band (instead of a simple curve), represented as a grey region on plots, that indicates an expectation area from the models that produce similar

**Table 1** Decay data of the radionuclides of interest [16]

| | Half-life | Energy of γ-radiation (keV) | Intensity of γ-radiation |
|---|---|---|---|
| $^{47}$Sc | 3.3492 d *6* | 159.381 *15* | 68.3% *4* |
| $^{46}$Sc | 83.79 d *4* | 889.277 *3* | 99.9840% *10* |
| $^{24}$Na | 14.997 h *12* | 1368.626 *5* | 99.9936% *15* |
| $^{57}$Ni | 35.60 h *6* | 1377.63 *3* | 81.7% *2.4* |

cross section results. Specifically, we have not included the version of the exciton model where the numerical transition rates are obtained with the optical model for collision probability (preeqmode = 3), as well as the complete quantum mechanical treatment via the Multi-Step Compound and Multi-Step Direct mechanisms (preeqmode = 4). In addition, for the same reason of retaining only those models without strong variability, for the level densities we have excluded the results obtained with the temperature-dependent Hartree–Fock-Bogolyubov calculations with the Gogny force (ldmodel = 6). The resulting band includes as special case the default calculation but excludes possible TALYS alternatives such as the one suggested by Duchemin et al. [18].

Table 2 reports the important models for pre-equilibrium and density levels used by the three codes. For both TALYS and EMPIRE, the global nucleon-nucleus optical potential of Koning-Delaroche [19] was used. For the α-nucleus optical model in EMPIRE, the potential used is specified by Avrigeanu et al. [20], while for TALYS the corresponding α-nucleus potential is determined in a more recent publication by Avrigeanu et al. [21]. Concerning the density levels, the relevant parameters for the EGSM level-density model in EMPIRE calculations can be found in the work by Capote et al. [22]. Instead, for TALYS, for which we considered a variety of models as specified in Table 2, the main level-density parameters for the models used can be found in the document by Koning et al. [23]. Finally, for FLUKA, we made reference to the publication by Ferrari and Sala [24], both for the definition of the optical models employed as well as for the main parameters of the level densities.

**Table 2** Pre-equilibrium (PE) and level density (LD) models used by the referenced codes [9–11]

| Code | PE Model | LD Model |
|---|---|---|
| TALYS | 1. Exciton (analytical)<br>2. Exciton (numerical)<br>3. Exciton + optical<br>4. MSD/MSC | 1. CT + FG<br>2. BSFG<br>3. GSFM<br>4. Microscopic (Goriely)<br>5. Microscopic (Hilaire)<br>6. T-dep HFB |
| EMPIRE | HMS | EGSM |
| FLUKA | PEANUT | Modified FG |

*MSD* multi-step direct, *MSC* multi-step compound, *CT* constant temperature, *FG* fermi gas, *BSFG* back shifted fermi gas, *GSFM* generalized superfluid model, *HFB* Hartree–Fock–Bogliubov, *HMS* hybrid Montecarlo simulation, *PEANUT* pre-equilibrium approach to nuclear thermalization, *EGSM* enhanced generalized superfluid model

## Results and discussion

Table 3 includes our new data for the $^{nat}V(p,x)^{47}Sc,^{46}Sc$ nuclear cross sections, as well as the values of the IAEA reference cross sections used. The uncertainty of the proton energy takes into account the uncertainty on the extracted proton beam (± 500 keV) and the energy straggling, calculated with SRIM, giving a maximum value of ± 800 keV (Table 3). Figures 1 and 2 reports our new data set (red dots), which are compared with EXFOR data [17]; it can be easily noted that the uncertainties of our data are smaller than those previously published, due to several γ-spectrometry acquisitions performed in this work.

The trend of the $^{nat}V(p,x)^{47}Sc$ cross section measured in this work agrees with previous data in the entire energy range (26.5–70.0 MeV), as shown in Fig. 1. The value at 60 MeV by Heininger and Wiig [25] is reported on the plot despite its

**Table 3** Data of the $^{nat}V(p,x)^{47}Sc,^{46}Sc$ nuclear cross sections and the values of the IAEA reference cross sections used [13]

| Energy $^{nat}V$ foil (MeV) | $^{47}Sc$ cross section (mb) | $^{46}Sc$ cross section (mb) | Reference radionuclide | Energy monitor foil (MeV) | Monitor cross section (mb) |
|---|---|---|---|---|---|
| 26.5 ± 0.8 | 4.3 ± 0.2 | | $^{57}Ni$ | 26.3 ± 0.9 | 180.2 ± 7.5 |
| 29.2 ± 0.8 | 7.4 ± 0.5 | | $^{57}Ni$ | 29.0 ± 0.8 | 162.9 ± 6.8 |
| 31.2 ± 0.7 | 9.0 ± 0.5 | 0.6 ± 0.1 | $^{57}Ni$ | 31.1 ± 0.7 | 136.6 ± 5.7 |
| 33.3 ± 0.6 | 10.9 ± 0.6 | 2.6 ± 0.2 | $^{57}Ni$ | 33.5 ± 0.6 | 113.9 ± 4.8 |
| 39.5 ± 0.6 | 8.3 ± 0.5 | 18.6 ± 1.1 | $^{57}Ni$ | 39.3 ± 0.6 | 85.6 ± 3.6 |
| 48.1 ± 0.8 | 4.6 ± 0.3 | 30.8 ± 2.4 | $^{24}Na$ | 48.1 ± 0.8 | 4.8 ± 0.3 |
| 51.0 ± 0.7 | 4.1 ± 0.3 | 27.8 ± 2.3 | $^{24}Na$ | 50.9 ± 0.7 | 6.4 ± 0.5 |
| 53.6 ± 0.6 | 4.1 ± 0.3 | 25.1 ± 2.0 | $^{24}Na$ | 53.7 ± 0.5 | 8.0 ± 0.6 |
| 55.7 ± 0.8 | 4.4 ± 0.4 | 23.0 ± 1.9 | $^{24}Na$ | 55.6 ± 0.8 | 9.0 ± 0.6 |
| 58.3 ± 0.7 | 5.0 ± 0.4 | 21.6 ± 1.8 | $^{24}Na$ | 58.2 ± 0.7 | 10.0 ± 0.7 |
| 60.7 ± 0.6 | 5.1 ± 0.3 | 18.6 ± 1.2 | $^{24}Na$ | 60.7 ± 0.5 | 10.8 ± 0.5 |
| 65.5 ± 0.8 | 6.8 ± 0.4 | 16.7 ± 1.0 | $^{24}Na$ | 65.5 ± 0.8 | 11.4 ± 0.5 |
| 67.8 ± 0.7 | 7.7 ± 0.5 | 16.7 ± 1.0 | $^{24}Na$ | 67.7 ± 0.7 | 11.6 ± 0.5 |
| 70.0 ± 0.6 | 8.0 ± 0.4 | 16.4 ± 0.9 | $^{24}Na$ | 70.0 ± 0.5 | 11.6 ± 0.4 |

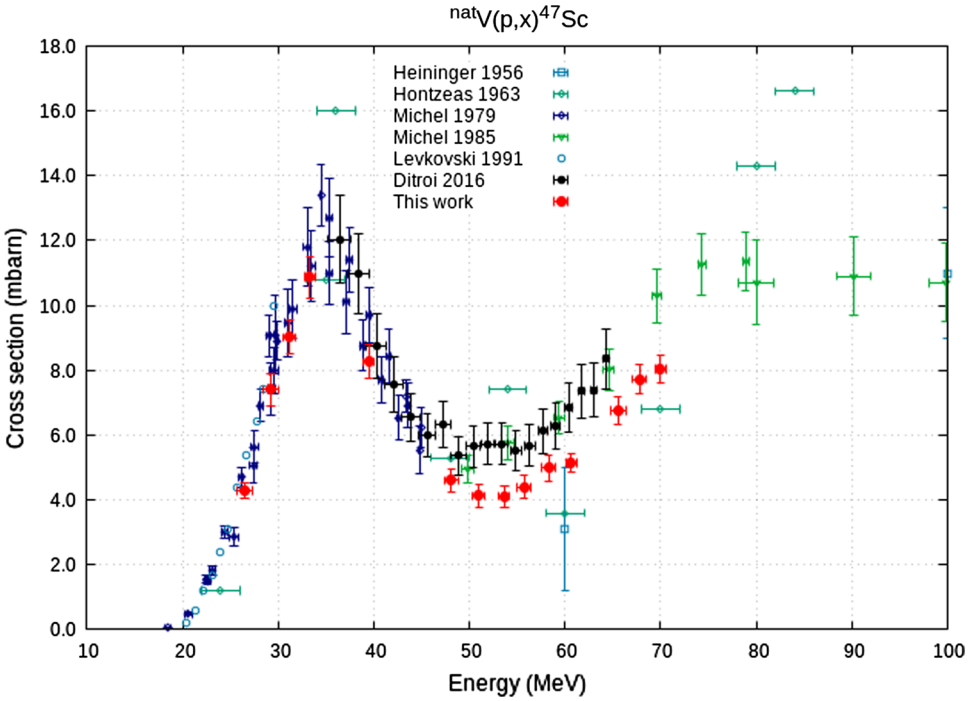


**Fig. 1** Experimental results of the $^{nat}V(p,x)^{47}Sc$ compared with previous data [17]

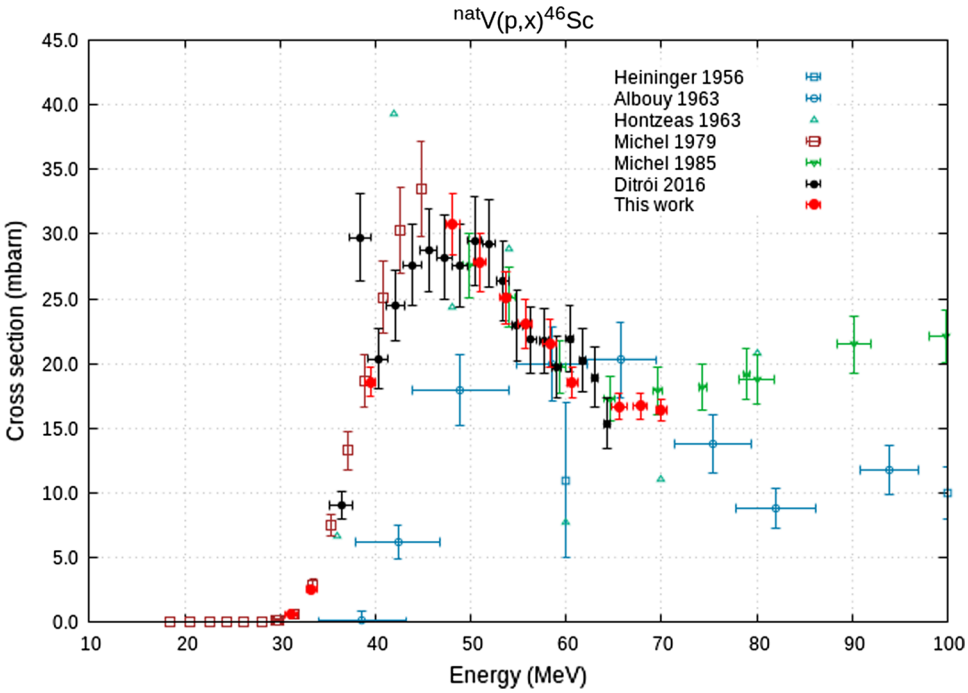


**Fig. 2** Experimental results of the $^{nat}V(p,x)^{46}Sc$ compared with previous data [17]

large uncertainty. The first bump of the $^{nat}V(p,x)^{47}Sc$ reaction around 35 MeV is due to the dominance, in the evaporation processes, of the (p,pα) channel (threshold energy on $^{51}V$ at 10.5 MeV, as shown in Table 4), while the second rise, starting at energies higher than 60 MeV, describes the emission in different channels (threshold energies reported in Table 4), related to secondary emissions such as (p,3p2n). The shape of the cross section in this region is strongly affected by the pre-equilibrium processes.

Figure 1 shows a good agreement of our data below 40 MeV with previous results by Michel et al. [26], Levkovski [27] and Ditrói et al. [28]. On the other hand, the cross section values obtained in this work at EP > 40 MeV are (20–30%) lower than previous data, published by Ditrói et al.

**Table 4** *Q*-values and threshold energies for $^{47}$Sc production with $^{51}$V as target [16]

| | *Q*-value (MeV) | Threshold energy (MeV) |
|---|---|---|
| p,p + α | − 10.292 | 10.496 |
| p,d + $^{3}$He | − 28.645 | 29.212 |
| p,2p + t | − 30.106 | 30.701 |
| p,n + p + $^{3}$He | − 30.870 | 31.480 |
| p,p + 2d | − 34.139 | 34.814 |
| p,n + 2p + d | − 36.363 | 37.082 |
| p,2n + 3p | − 38.588 | 39.351 |

[28] and Michel et al. [29]. The use of a different monitor reaction at energies higher than 40 MeV cannot be a possible explanation of such discrepancy since the natV(p,x)$^{46}$Sc cross section is in agreement with those data (Fig. 2). In particular, Michel et al. [29] used the $^{27}$Al(p,3p3n)$^{22}$Na reaction published in the CEA-N-1466(3) report by Tobailem and de Lassus St. Genies [30]. Ditrói et al. [28] used the same nuclear reaction $^{27}$Al(p,x)$^{24}$Na considered as reference of this work, but their results were published earlier than the update of the IAEA recommended cross sections occurred in August 2017.

The measurement of the $^{nat}$V(p,x)$^{46}$Sc cross section carried out in this work is in good agreement with previous data, including the ones by Ditrói et al. [28] and Michel et al. [27], up to 70 MeV (Fig. 2). A mismatch with current data is instead clearly shown in the estimations performed at 60 MeV by Heininger and Wiig [25] and the trend measured by Albouy [31], albeit they refer to older measurements having quite large error bars.

In Figs. 3 and 4 our new data are compared with the results from theoretical model calculations. In Fig. 3 the measured $^{47}$Sc production falls within the TALYS band, while the results from EMPIRE calculations overestimate the cross section by a factor of about 2; however, the energy dependence is correctly reproduced. The staggering behaviour of the EMPIRE results at high energy are due to the Montecarlo Module adopted (HMS) for pre-equilibrium. FLUKA results seem to offset the low-energy behavior around threshold (where the centrifugal and Coulomb barriers affect the cross-section) and slightly underestimate the cross section between 30 and 60 MeV.

Concerning Fig. 4, EMPIRE shows a behavior similar to that presented in Fig. 3, namely an overall overestimation by a factor around 2, but with a correct reproduction of the energy dependence. In the case of $^{46}$Sc, FLUKA better reproduces the general trend, except again moderately around the threshold region where there is an offset similar to that noticed in the previous figure. The TALYS band covers the experimental data up to the peak at 42 MeV, and then slightly underestimates the new data.

In Fig. 5 we report the ratio between the cross sections for $^{47}$Sc and the sum of both $^{47}$Sc and $^{46}$Sc. This ratio may be used to indicate the energy regions where the $^{47}$Sc production is possible with smallest contamination by $^{46}$Sc. These energy intervals correspond to a value of the ratio close to unity and represent good candidates for high-purity

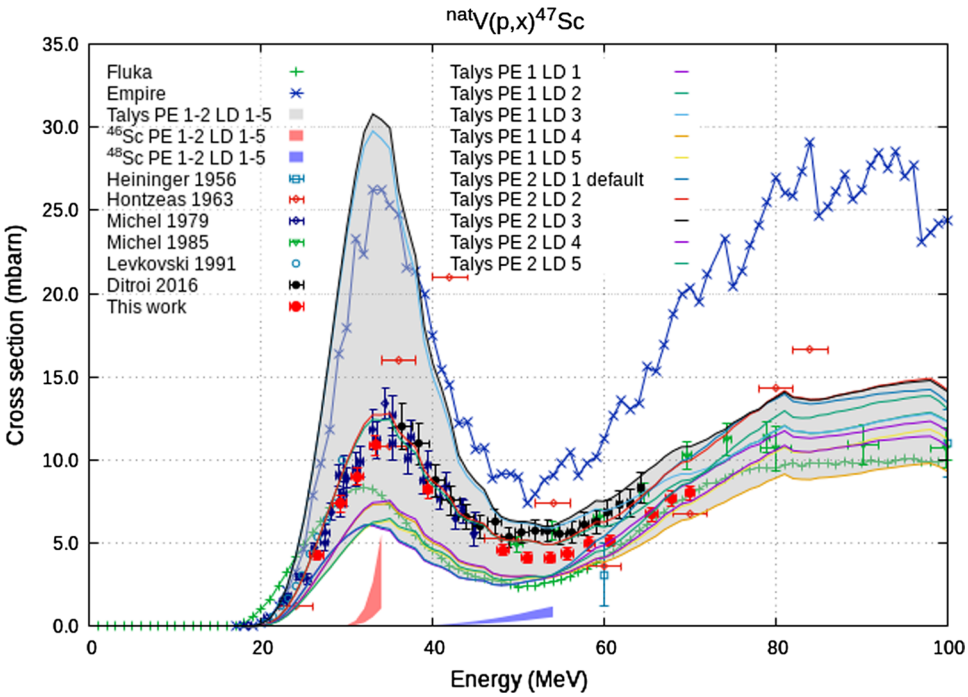


**Fig. 3** Theoretical calculations of the $^{nat}$V(p,x)$^{47}$Sc cross section compared with experimental results [17]. The initial trends of the $^{nat}$V(p,x)$^{46}$Sc, $^{48}$Sc cross sections, calculated with the TALYS code, are also shown

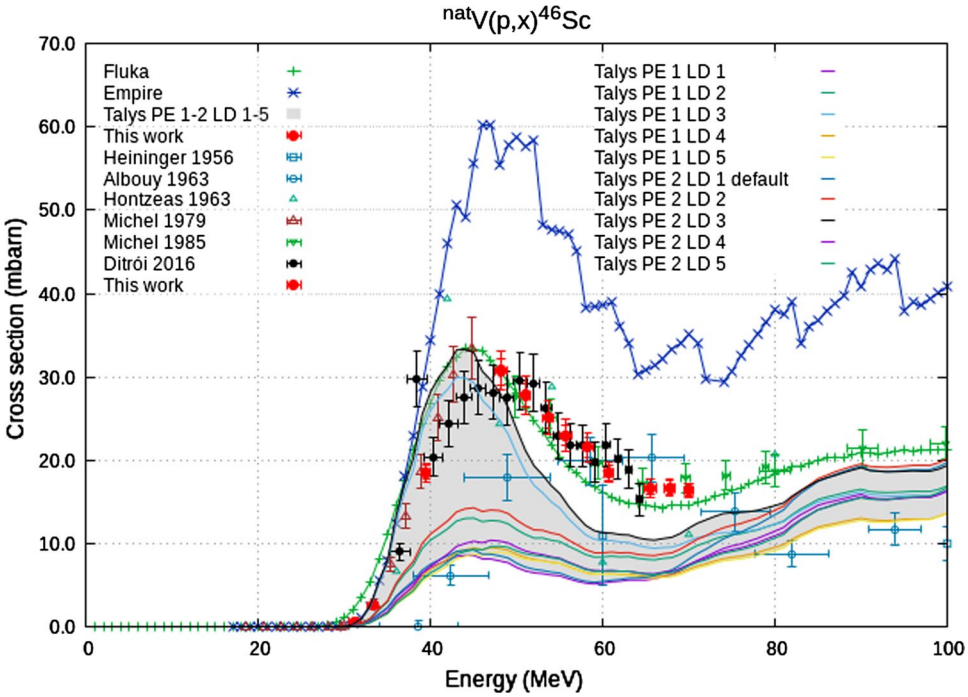


**Fig. 4** Theoretical calculations of the $^{nat}V(p,x)^{46}Sc$ cross section compared with experimental results [17]

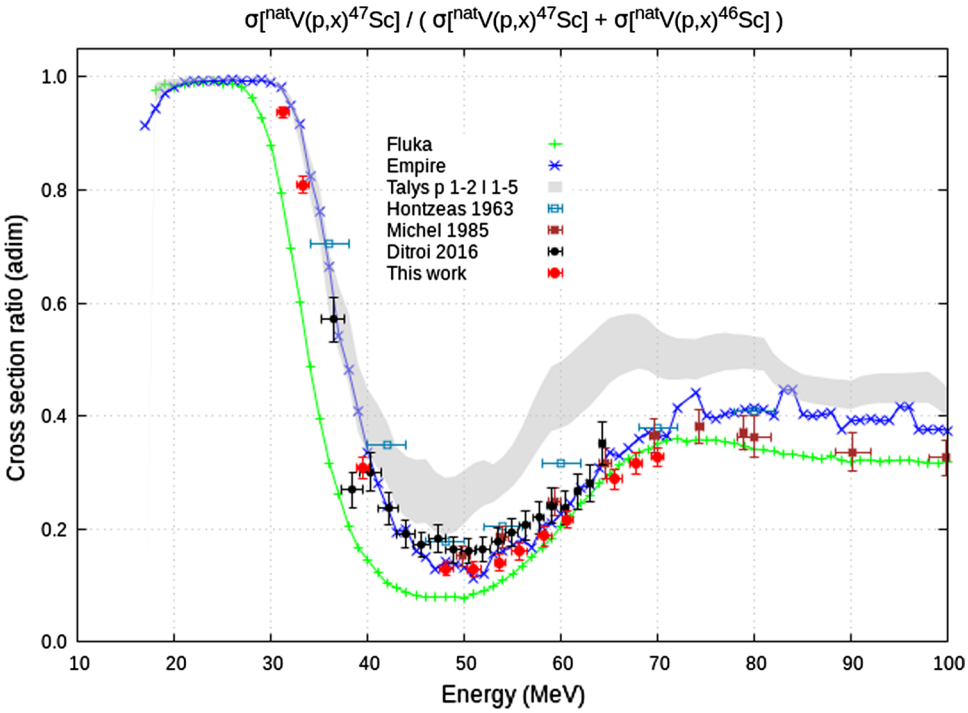


**Fig. 5** Cross section ratio between $^{47}Sc$ production and $^{46}Sc$ plus $^{47}Sc$; the ratio obtained with measured data within this work is also reported with red dots

productions. In the figure we have selected the subset of experimental data presented in this work and in the available literature [17], where both radionuclides were measured at the same energy and full error propagation was taken into account, accordingly. It is interesting to observe that in comparison with the absolute cross section values, in case of this ratio the variability of theoretical calculations is much reduced.. In particular, calculations with the EMPIRE code, whose data appeared somewhat more distant from the experimental ones (Figs. 3, 4), have indeed shown the best agreement about such a ratio at all the energies explored. Also other calculations are not far from the data. The FLUKA results confirm a good reproduction but with an offset at low energy, as already observed in the previous figures. The

band of TALYS appears very narrow, indicating that significant differences in the specific TALYS model considered are compressed when one considers the ratio of the two cross sections.. The thresholds region is very well reproduced, like in the EMPIRE code, but a slight offset in the ratio appears at about 50 MeV and above. At last, taking into account all the considerations here reported, it may be inferred that there is a region (below 30 MeV) where $^{47}$Sc radionuclide may be produced with practically no $^{46}$Sc. The estimation of the Thick Target Yield (TTY) was performed for $^{47}$Sc and $^{46}$Sc radionuclides by considering a polynomial fit of the experimental data, to obtain an expression of the dependence of the cross section as a function of the proton energy. Experimental data included in the fit were both the values available on the EXFOR database and the new ones measured in this work. In this interesting energy range (19–30 MeV) the production of $^{47}$Sc is calculated to be 31 MBq/μA and 82 MBq/μA for 24 h and 80 h irradiation runs respectively; in these irradiation conditions the co-production of $^{46}$Sc can be considered negligible, respectively 0.01 MBq/μA and 0.03 MBq/μA. It would be of great importance to measure the TTY in this energy region to prove that $^{47}$Sc can be produced with a very high purity level from $^{nat}$V and low-energy proton cyclotrons ($E_P \leq 30$ MeV).

## Conclusions

This work describes the cross sections measurements of the $^{nat}$V(p,x)$^{47}$Sc, $^{46}$Sc nuclear reactions carried out during the PASTA project, in collaboration with the Arronax facility. Sets of $^{nat}$V target foils, arranged in stacked-foils structures, were bombarded by the proton beam up to 70 MeV. Results obtained in the six irradiation runs, carried out during 2017 and 2018, are in perfect agreement, despite the year standing between measurements and indicating that the experiment is under control. Results obtained in this work have smaller uncertainties than previous data thanks to the repetition of γ-spectrometry acquisitions performed for each $^{nat}$V foil. In comparison with the previous measurements, a general good agreement in the trend of both nuclear reactions was obtained. However, in the case of the $^{nat}$V(p,x)$^{47}$Sc cross section and for $E_P > 40$ MeV, a discrepancy up to 30% with the data published by Ditròi et al. [28] and by Michel et al. [29] was noted. Our experimental values were also compared with theoretical calculations obtained by using three nuclear codes, namely TALYS, EMPIRE and FLUKA. For both radionuclides, the trend of the theoretical estimations is in good agreement with the experimental data; however, an overestimation of a factor of about 2 can be noted on the peak values. Results form all the theoretical codes agree on a low energy window ($E_P \leq 30$ MeV) where $^{47}$Sc is produced with no contamination by $^{46}$Sc. This is particularly interesting as production route for preclinical studies (in vitro and in vivo), considering the low-cost, easy available $^{nat}$V targets and the widespread number of medium energy proton cyclotrons. This work suggests that this production route deserves attention and a thorough investigation involving also other relevant contaminants (such as $^{48}$Sc and the stable $^{45}$Sc). In addition, dosimetric calculations may support the identification of the best irradiation parameters to produce $^{47}$Sc for theranostic applications, providing the maximum tolerable amount of radioisotopic impurities (especially $^{46}$Sc). Further work on this topic is currently underway.

**Acknowledgements** The authors thanks Dr. R. Capote, Dr. M. W. Herman, and Dr. Carlos Rossi Alvarez for private communications and the enlightening scientific discussion. This work has been partially supported by EU Horizon 2020 Project RIA-ENSAR2 (654 02) and by a Grant from the French National Agency for Research called "Investissements d'Avenir", Equipex Arronax-Plus noANR-11-EQPX-0004, Labex IRON noANR-11-LABX-18-01 and noANR-16-IDEX-0007.

**Funding** Funding was provided by Istituto Nazionale di Fisica Nucleare CSN5 with the Grant PASTA (Bando Giovani Ricercatori No. 18203).

## Compliance with ethical standards

**Conflict of interest** The authors declare that they have no conflict of interest.

## References

1. Qaim SM, Scholten B, Neumaier B (2018) J Radioanal Nucl Chem. https://doi.org/10.1007/s10967-018-6238-x
2. IAEA, CRP on therapeutic radiopharmaceuticals labelled with new emerging radionuclides ($^{67}$Cu, $^{186}$Re, $^{47}$Sc), No. F22053, 2016-2020. http://cra.iaea.org/cra/explore-crps/all-active-by-programme.html
3. Müller C, Domnanich KA, Umbricht CA, Van Der Meulen NP (2018) Scandium and terbium radionuclides for radiotheranostics: current state of development towards clinical applications. Br J Radiol. https://doi.org/10.1259/bjr.20180074
4. Champion C, Quinto MA, Morgat C, Zanotti-Fregonara P, Hindié E (2016) Comparison between three promising ß-emitting radionuclides, $^{67}$Cu, $^{47}$Sc and $^{161}$Tb, with emphasis on doses delivered to minimal residual disease. Theranostics. https://doi.org/10.7150/thno.15132
5. Boschi A, Martini P, Costa V, Pagnoni A, Uccelli L (2019) Interdisciplinary tasks in the cyclotron production of radiometals for medical applications. The case of $^{47}$Sc as example. Molecules. https://doi.org/10.3390/molecules24030444
6. Huclier-Markai S, Alliot C, Kerdjoudj R, Mougin-Degraef M, Chouin N, Haddad F (2018) Promising scandium radionuclides for nuclear medicine: a review on the production and chemistry up to in vivo proofs of concept. Cancer Biother Radio. https://doi.org/10.1089/cbr.2018.2485

7. Esposito J et al (2019) LARAMED: a laboratory for radioisotopes of medical interest. Molecules. https://doi.org/10.3390/molecules24010020
8. Haddad F et al (2008) ARRONAX, a high-energy and high-intensity cyclotron for nuclear medicine. Nucl Med Mol Imaging. https://doi.org/10.1007/s00259-008-0802-5
9. Koning AJ, Hilarie S, Duijvesijn MC (2008) TALYS.1.0. In: Proceeding of the international conference on nuclear data for science and technology, April 22–27, 2007, Nice, France, EDP Sciences, p 211
10. Herman M et al (2007) EMPIRE: nuclear reaction model code system for data evaluation. Nucl Data Sheets 108:2655
11. Boehlen TT et al (2014) The FLUKA code: developments and challanges for high energy and medical applications. Nucl Data Sheets 120:211
12. Pupillo G et al (2018) New production cross sections for the theranostic radionuclide $^{67}$Cu. Nuclear Instr Methods Phys Res B. https://doi.org/10.1016/j.nimb.2017.10.022
13. IAEA Monitor Reactions (2017) https://www-nds.iaea.org/medical/monitor_reactions.html. Accessed Mar 2019
14. Ziegler JF, Ziegler MD, Biersack JP (2010) SRIM—the stopping and range of ions in matter. Nuclear Instr Methods Phys Res B 268:1818–1823
15. Otuka N et al (2017) Uncertainty propagation in activation cross section measurements. Radiat Phys Chem. https://doi.org/10.1016/j.radphyschem.2017.01.013
16. National Nuclear Data Center (NNDC), NuDat 2.7 database. https://www.nndc.bnl.gov/. Accessed Mar 2019
17. Experimental Nuclear Reaction Data (EXFOR). https://www-nds.iaea.org/exfor/exfor.htm. Accessed Mar 2019
18. Duchemin C, Guertin A, Haddad F, Michel N, Métivier V (2015) Production of medical isotopes from a thorium target irradiated by light charged particles up to 70 MeV. Phys Med Biol. https://doi.org/10.1088/0031-9155/60/3/931
19. Koning AJ, Delaroche JP (2003) Local and global nucleon optical models from 1 keV to 200 MeV. Nucl Phys A 713:231
20. Avrigeanu V, Hodgson PE, Avrigeanu M (1994) Global optical potentials for emitted alpha particles. Phys Rev C 49:2136
21. Avrigeanu V et al (2014) Further explorations of the α-particle optical model potential at low energies for the mass range $A \approx 45–209$. Phys Rev C 90:044612
22. Capote R et al (2009) Reference input parameter library for calculation of nuclear reactions and nuclear data evaluations. Nucl Data Sheets 110:3107–3214
23. Koning A, Hilaire S, Goriely S (2017) TALYS-1.9 user manual
24. Ferrari A and Sala PR (1998) The physics of high energy reactions. In: Gandini A, Reffo G (eds) Proceedings of the workshop on nuclear reaction data and nuclear reactors physics, design and safety, International Centre for Theoretical Physics, Miramare-Trieste, Italy, 15 April–17 May 1996. World Scientific, p 424
25. Heininger CG and Wiig EO (1956) Spallation of Vanadium with 60-, 100-, 175-, and 240-MeV protons. Phys Rev 101:1074
26. Michel R, Brinkmann G, Weigel H and Herr W (1979) Measurement and hybrid-model analysis of proton-induced reactions with V, Fe, and Co. Nucl Phys, Sect A 322:40
27. Levkovski VN (1991) Activation cross sections by protons and alphas, Moscow, USSR
28. Ditrói F, Tárkányi F, Takács S, Hermanne A (2016) Nuclear Instr Methods Phys Res B 381:16–28
29. Michel R, Stueck R, Peiffer F (1985) Proton-induced reaction on Ti, V, Mn, Fe, Co and Ni. Nucl Phys, Sect A 441:617
30. Tobailem J and de Lassus St. Genies CH (1975) report CEA-N-1466(3)
31. Albouy G, Cohen JP, Gusakow M, Poffe N, Sergolle H and Valentin L (1963) Reaction (p,3n+3p) between 30 and 150 MeV. J de Physique 24:67